Bond-orbital models for superlattices

Yia-Chung Chang
Department of Physics and Materials Research Laboratory, University of Illinois at Urbana-Champaign, 1110 West Green Street, Urbana, Illinois 61801
(Received 30 October 1987)

A simple theoretical method for calculating superlattice electronic structures based on the bond-orbital model is presented. The method combines the virtues of the envelope-function ($\mathbf{k}\cdot\mathbf{p}$) and tight-binding methods. The method contains no fitting parameters; all interaction parameters involved are directly related to parameters for describing bulk bands near the zone center in the $\mathbf{k}\cdot\mathbf{p}$ perturbation theory. Subband structures of a GaAs-$Al_xGa_{1-x}As$ and an InAs-GaSb superlattice are calculated for illustration.

I. INTRODUCTION

Research interest in the area of semiconductor superlattices[1] has grown tremendously during the past few years. Many theoretical methods[2–21] have been developed for calculating the electronic structures of superlattices. These theoretical methods can be classified into three categories: the pseudopotentials,[2–4] the tight binding,[5–11] and the envelope-function ($\mathbf{k}\cdot\mathbf{p}$) (Refs. 12–21) methods. Among these methods, the envelope-function approach is most widely adopted because of its simplicity. With various refinements,[16–21] this approach can become quite sophisticated and can be used to study many problems such as band mixing, the effects of external fields (modulation doping, electric field, magnetic field, and unaxial stress, etc.), impurities, and exciton states. The major drawback of this method is that the boundary conditions become extremely complicated when many bands are involved.[15,19] The tight-binding method requires more computational effort. However, it takes the effect of full band structure into account, and the boundary conditions for connecting superlattice wave functions across the interface in this model are straightforward. The main disadvantage of the tight-binding model is that it requires many empirical parameters which are usually determined by tedious fitting procedures. In this paper, we introduce yet another theoretical method which is closely related to the envelope-function and the tight-binding methods. In fact, this method may be considered as a link between the above two methods. The method is based on the bond-orbital model.[22] The computational effort required to implement this method is comparable to the envelope-function method involving the same number of bands. In addition, the method contains many virtues of the empirical tight-binding method, while avoiding the tedious fitting procedure.

The basic idea of this method is to use a minimum number of bond orbitals to describe, as accurately as possible, the most relevant portion of the band structure for the bulk materials which constitute the superlattice. For example, to calculate the valence-subband structures of a GaAs-$Al_xGa_{1-x}As$ superlattice, the minimum information needed is the energy dispersion of the top four valence bands near the zone center for GaAs and $Al_xGa_{1-x}As$. In this case, four bond orbitals per unit cell (made of p-like states coupled with spin to form orbitals with total angular momentum $J=\frac{3}{2}$) are used to obtain the top four valence bands for each bulk material. For narrow-gap semiconductors, such as HgTe, InSb, InAs, etc., we have to add two s-like bond orbitals (with spin up and down) per unit cell to describe the lowest two conduction bands (including the spin degeneracy), since the superlattice states of interest contain admixtures of both the valence-band and conduction-band characters. In cases where the split-off band is also of importance, we also need to include two additional bond orbitals per unit cell (made of p-like states coupled with spin to form orbitals of total angular momentum $J=\frac{1}{2}$). We shall assume that all these bond orbitals are sufficiently localized so that the interaction between orbitals separated farther than the nearest neighbor distance can be ignored. All nonvanishing interaction parameters can then be directly related to the effective masses or other band parameters obtained in the $\mathbf{k}\cdot\mathbf{p}$ perturbation theory. The relation is determined by requiring the band structures of relevant bulk materials obtained by this method to be identical to those predicted by the $\mathbf{k}\cdot\mathbf{p}$ theory up to the second order in $\mathbf{k}$.

II. BOND-ORBITAL MODELS

We first consider a valence-band model (VBM), in which only the top three valence bands (in the absence of spin-orbit interaction) are included. This model requires only three p-like bond orbitals (labeled x,y,z) per unit cell. Here a bond orbital is defined as the proper linear combination of two atomic orbitals within a unit cell of a diamond or zinc-blende crystal which best describe the valence-band states near the zone center. We denote an α-like ($\alpha=x,y,z$) bond orbital localized at lattice site $\mathbf{R}$ as $|\mathbf{R},\alpha\rangle$. The interaction between orbitals $|\mathbf{R},\alpha\rangle$ and $|\mathbf{R}',\alpha'\rangle$ for a face-centered-cubic lattice is given by[23]

$$\langle \mathbf{R},\alpha \mid H \mid \mathbf{R}',\alpha' \rangle = E_p \delta_{\mathbf{R},\mathbf{R}} \delta_{\alpha,\alpha'} + \delta_{\mathbf{R}'-\mathbf{R},\tau} \{ E_{xy} \tau_\alpha \tau_{\alpha'} (1-\delta_{\alpha,\alpha'}) + [E_{xx} \tau_\alpha^2 + E_{zz}(1-\tau_\alpha^2)] \delta_{\alpha,\alpha'} \} , \tag{1}$$

where E_p denotes the on-site energy and E_{xx}, E_{xy}, and E_{zz} are three independent nearest-neighbor interaction parameters. Here $E_{\alpha,\alpha'}$ denotes the interaction between an α-like orbital at the origin and an α'-like orbital located at $(1,1,0)(a/2)$, a being the lattice constant. The remaining interaction parameters can be related to E_{xx}, E_{xy}, and E_{zz} by symmetry. τ_α denote the α component of the twelve nearest-neighbor position vectors in units of $(a/2)$,

$$\tau = (\pm 1, \pm 1, 0),\ (\pm 1, 0, \pm 1),\ (0, \pm 1, \pm 1) .$$

The top three valence bands (in the absence of spin-orbit interaction) of a typical zinc-blende or diamond crystal can be obtained by diagonalizing the tight-binding Hamiltonian

$$H_{\alpha,\alpha'}(\mathbf{k}) = E_p \delta_{\alpha,\alpha'} + \sum_\tau e^{i\mathbf{k}\cdot\tau} \{ E_{xy} \tau_\alpha t_{\alpha'} + [(E_{xx} - E_{xy})\tau_\alpha^2 + E_{zz}(1-\tau_\alpha^2)] \delta_{\alpha,\alpha'} \} . \tag{2}$$

Taking the Taylor expansion over $\mathbf{k}$ and omitting terms higher than the second order, we obtain

$$H(\mathbf{k}) = \begin{bmatrix} E_v - \lambda_1 k_x^2 - \lambda_2 k^2 & -\lambda_3 k_x k_y & -\lambda_3 k_x k_z \\ -\lambda_3 k_x k_y & E_v - \lambda_1 k_y^2 - \lambda_2 k^2 & -\lambda_3 k_y k_z \\ -\lambda_3 k_x k_z & -\lambda_3 k_y k_z & E_v - \lambda_1 k_z^2 - \lambda_2 k^2 \end{bmatrix} , \tag{3}$$

where

$$\begin{aligned} E_v &= E_p + 8E_{xx} , \\ \lambda_1 &= (E_{zz} - E_{xx}) a^2/2 , \\ \lambda_2 &= (3E_{xx} - E_{zz}) a^2/2 , \\ \lambda_3 &= E_{xy} a^2 . \end{aligned} \tag{3'}$$

Comparing $H(\mathbf{k})$ with the $\mathbf{k}\cdot\mathbf{p}$ Hamiltonian for the valence bands, we have

$$(L-M) = \lambda_1,\ M = \lambda_2,\ N = \lambda_3 , \tag{4}$$

where L, M, and N are $\mathbf{k}\cdot\mathbf{p}$ band parameters defined in Ref. 24. The above equations provide a one-to-one correspondence between the band parameters L, M, and N (measurable by the cyclotron-resonance experiment[25]) and the bond-orbital interaction parameters E_{xx}, E_{xy}, and E_{zz}. The on-site energy E_p plays the role of adjusting the energy position of the valence-band top (E_v).

For most semiconductors of interest, the spin-orbit interaction is important. Thus we choose the proper linear combinations of the product of the electron spin and the three p-like orbitals as the new bond-orbital basis. The spin-orbit coupled bond orbitals (SOBO's) can be written as

$$| \mathbf{R}, u_M^J \rangle = \sum_{\alpha,\sigma} C(\alpha\sigma; JM) | \mathbf{R},\alpha \rangle \chi_\sigma , \tag{5}$$

where $J = \frac{3}{2}, \frac{1}{2}$, $M = -J, \ldots, J$, and χ_σ, $\sigma = \frac{1}{2}, -\frac{1}{2}$ denote the electron spinors. The coupling coefficients $C(\alpha,\sigma;JM)$ are given in Table I. By including the spin-orbit interaction, we obtain the tight-binding Hamiltonian in the new SOBO basis as

$$\begin{aligned} H_{JM,J'M'}(\mathbf{k}) = {} & (J - \tfrac{3}{2}) \Delta \delta_{JM,J'M'} \\ & + \sum_{\alpha,\alpha',\sigma} C^*(\alpha\sigma; JM) C(\alpha'\sigma; J'M') \\ & \times H_{\alpha,\alpha'}(\mathbf{k}) , \end{aligned} \tag{6}$$

where Δ is the spin-orbit splitting. Taking the Taylor expansion over $\mathbf{k}$ and omitting terms higher than the second order in $\mathbf{k}$, we immediately obtain the Kohn-Luttinger Hamiltonian.[26] There is a one-to-one correspondence between the Luttinger parameters, γ_1, γ_2, and γ_3 and the bond-orbital interaction parameters E_{xx}, E_{xy}, and E_{zz}. The relations are given in Table II in the column labeled VBM.

Next we consider a model for describing the coupling of the lowest conduction band and the top three valence bands. We shall refer to this model as the coupled

TABLE I. Coupling coefficients for p-like states coupled to the electron spin.

(J,M) \ (α,σ)	$(x,\frac{1}{2})$	$(y,\frac{1}{2})$	$(z,\frac{1}{2})$	$(x,-\frac{1}{2})$	$(y,-\frac{1}{2})$	$(z,-\frac{1}{2})$
$(\frac{3}{2},\frac{1}{2})$	$-1/\sqrt{2}$	$-i/\sqrt{2}$	0	0	0	0
$(\frac{3}{2},\frac{1}{2})$	0	0	$2/\sqrt{6}$	$-1/\sqrt{6}$	$i/\sqrt{6}$	0
$(\frac{3}{2},-\frac{1}{2})$	$1/\sqrt{6}$	$i/\sqrt{6}$	0	0	0	$2/\sqrt{6}$
$(\frac{3}{2},-\frac{3}{2})$	0	0	0	$1/\sqrt{2}$	$-i/\sqrt{2}$	0
$(\frac{1}{2}),\frac{1}{2})$	0	0	$-1/\sqrt{3}$	$-1/\sqrt{3}$	$-i/\sqrt{3}$	0
$(\frac{1}{2},-\frac{1}{2})$	$-1/\sqrt{3}$	$i/\sqrt{3}$	0	0	0	$1/\sqrt{3}$

TABLE II. Relations between bond-orbital parameters and $\mathbf{k}\cdot\mathbf{p}$ parameters. $R_0=\hbar^2/2m_0a^2$, $X_{hl}=4$ eV.

VBM	CVBM
	$E_{sx}^2=E_g(12\gamma_2R_0-X_{hl}/8)/32$
$E_{xy}=6\gamma_3R_0$	$E_{xy}=6\gamma_3R_0-16E_{sx}^2/E_g$
$E_{xx}=(\gamma_1+4\gamma_2)R_0$	$E_{xx}=\gamma_1R_0-16E_{sx}^2/(3E_g)+X_{hl}/24$
$E_{zz}=(\gamma_1-8\gamma_2)R_0$	$E_{zz}=E_{xx}+X_{hl}/8$
$E_p=E_v-12\gamma_1R_0$	$E_p=E_v-12E_{xx}+X_{hl}/2$
	$E_{ss}=-\frac{m_0}{m_c}R_0+64E_{sx}^2\left[\frac{2}{E_g}+\frac{1}{E_g+\Delta}\right]/3$

conduction–valence-band model (CVBM). Such a model is needed for treating superlattices like InAs-GaSb and HgTe-CdTe, in which the mixing of conduction-band and valence-band states is of importance. In this model we include one s-like and three p-like bond orbitals per unit cell. In addition to the tight-binding matrix elements given in (1), we also have

$$\langle \mathbf{R},s \mid H \mid \mathbf{R}',s\rangle=E_s\delta_{\mathbf{R}',\mathbf{R}}+E_{ss}\delta_{\mathbf{R}'-\mathbf{R},\tau} \tag{7}$$

and

$$\langle \mathbf{R},s \mid H \mid \mathbf{R},\alpha\rangle=E_{sx}\delta_{\mathbf{R}'-\mathbf{R},\tau}\tau_\alpha\ , \tag{8}$$

where $\mid \mathbf{R},s\rangle$ denote an s-like orbital located at $\mathbf{R}$. Taking the Taylor expansion over $\mathbf{k}$ and omitting terms higher than the second order in $\mathbf{k}$, we obtain the Hamiltonian in the sp^3 basis

$$H(\mathbf{k})=\begin{bmatrix} E_c-E_{ss}a^2k^2 & i4E_{sx}ak_x & i4E_{sx}ak_y & i4E_{sx}ak_z \\ -i4E_{sx}ak_x & E_v-\lambda_1k_x^2-\lambda_2k^2 & -\lambda_3k_xk_y & -\lambda_3k_xk_z \\ -i4E_{sx}ak_y & -\lambda_3k_xk_y & E_v-\lambda_1k_y^2-\lambda_2k^2 & -\lambda_3k_yk_z \\ -i4E_{sx}ak_z & -\lambda_3k_xk_z & -\lambda_3k_yk_z & E_v-\lambda_1k_z^2-\lambda_2k^2 \end{bmatrix}, \tag{9}$$

where E_v, λ_1, λ_2, and λ_3 are defined identically as in (3′), and $E_c=E_s+12E_{ss}$. If we block diagonalize the matrix $H(\mathbf{k})$ so that the conduction band and the valence bands are decoupled, the new Hamiltonian matrix correct to second order in $\mathbf{k}$ reads

$$H(\mathbf{k})=\begin{bmatrix} E_c+(\lambda_4-E_{ss}a^2)k^2 & 0 & 0 & 0 \\ 0 & E_v-(\lambda_1+\lambda_4)k_x^2-\lambda_2k^2 & -(\lambda_3+\lambda_4)k_xk_y & -(\lambda_3+\lambda_4)k_xk_z \\ 0 & -(\lambda_3+\lambda_4)k_xk_y & E_v-(\lambda_1+\lambda_4)k_y^2-\lambda_2k^2 & -(\lambda_3+\lambda_4)k_yk_z \\ 0 & -(\lambda_3+\lambda_4)k_xk_z & -(\lambda_3+\lambda_4)k_yk_z & E_v-(\lambda_1+\lambda_4)k_z^2-\lambda_2k^2 \end{bmatrix}, \tag{10}$$

where $\lambda_4=(4E_{sx}a)^2/E_g$, and $E_g=E_c-E_v$ denotes the band gap. Comparing (10) with the $\mathbf{k}\cdot\mathbf{p}$ theory of Ref. 24, we then obtain

$$\begin{aligned} &(L-M)=\lambda_1+\lambda_4,\ M=\lambda_2\ , \\ &N=\lambda_3+\lambda_4,\ \frac{\hbar^2}{2m_c}=\lambda_4-E_{ss}a^2\ . \end{aligned} \tag{11}$$

where m_c denotes the conduction-band effective mass. Note that in the above equations, the bond-orbital parameters are not uniquely related to the $\mathbf{k}\cdot\mathbf{p}$ parameters because we have four equations but five unknowns (E_{ss}, λ_1, λ_2, λ_3, and λ_4). Thus we need to impose an additional constraint. One obvious constraint is to require the matrix element describing the coupling between the conduction- and valence-band states near Γ to be the same as that given in the $\mathbf{k}\cdot\mathbf{p}$ theory, i.e.,

$$i4E_{sx}a=\frac{\hbar}{m_0}\langle S \mid P_x \mid X\rangle\ ,$$

where $\langle S \mid P_x \mid X\rangle$ is the momentum matrix element defined in Ref. 27. Although this constraint is quite physical, it sometimes leads to spurious valence-band structures in the CVBM. In particular, the light-hole band tends to cross the heavy-hole band at some finite wave vectors. To ensure that such crossing does not happen, we impose the constraint that the energy difference between the heavy-hole band and the light-hole band at X (denoted X_{hl}) obtained by the CVBM to be approximately the same as the value predicted by the empirical pseudopotential theory. In the CVBM it can be shown that this energy difference (X_{hl}) is just $8(E_{zz}-E_{xx})$. For most semiconductors of interest, this energy difference is about 4 eV. Thus we choose the constraint

$$(E_{zz}-E_{xx})=X_{hl}/8=0.5\text{ eV}\ . \tag{12}$$

TABLE III. Comparison of $16E_{sx}^2/R_0$ ($R_0=\hbar^2/2m_0a^2$) predicted the CVBM and $(2/m_0)\mid\langle S \mid P_x \mid X\rangle\mid^2$ predicted by the $\mathbf{k}\cdot\mathbf{p}$ theory (Ref. 27). The units are eV.

Material	$16E_{sx}^2/R_0$	$\frac{2}{m_0}\mid\langle S \mid P_x \mid X\rangle\mid^2$
GaAs	15.9	25.7
AlAs	7.98	21.1
InAs	20.1	22.2
GaSb	17.6	22.4
HgTe	19.3	18.0
CdTe	13.7	20.7

A comparison of $16E_{sx}^2/R_0$ ($R_0=\hbar^2/2m_0a^2$) predicted in the CVBM and $(2/m_0)|\langle S|P_x|X\rangle|^2$ predicted in the $\mathbf{k}\cdot\mathbf{p}$ theory[27] for a number of semiconductors is shown in Table III. We found that with this constraint $(E_{zz}-E_{xx})=0.5$ eV, the condition $i4E_{sx}a=(\hbar/m_0)\langle S|P_x|X\rangle$ is still approximately satisfied for narrow-gap semiconductors (e.g., InAs and HgTe) in which the coupling between the conduction and valence band is important.

Finally, we include the spin-orbit interaction in the CVBM. We define the s-like spin-orbit coupled bond orbitals located at $\mathbf{R}$ as

$$|\mathbf{R},\omega_\sigma\rangle=|\mathbf{R},s\rangle\chi_\sigma\ .$$

The p-like SOBO's are just $|\mathbf{R},u_M^J\rangle$ as defined in (5). The tight-binding Hamiltonian correct to the second order in $\mathbf{k}$ [in the basis $(\omega_{1/2},\omega_{-1/2},u_{3/2}^{3/2},u_{1/2}^{3/2},u_{-1/2}^{3/2},u_{-3/2}^{3/2},u_{1/2}^{1/2},u_{-1/2}^{1/2})$] can be written as

$$H(\mathbf{k})=\begin{pmatrix}
R' & 0 & S & T & S^*/\sqrt{3} & 0 & -T/\sqrt{2} & -\sqrt{2/3}S^* \\
0 & R' & 0 & S/\sqrt{3} & T & S^* & \sqrt{2/3}S & T/\sqrt{2} \\
S^* & 0 & P'+Q' & B' & C' & 0 & -B'/\sqrt{2} & -\sqrt{2}C' \\
T^* & S^*/\sqrt{3} & B'^* & P'-Q' & 0 & C' & \sqrt{2}Q' & \sqrt{3/2}B' \\
S/\sqrt{3} & T^* & C'^* & 0 & P'-Q' & -B' & \sqrt{3/2}B'^* & -\sqrt{2}Q' \\
0 & S & 0 & C'^* & -B'^* & P'+Q' & \sqrt{2}C' & -B'^*/\sqrt{2} \\
-T^*/\sqrt{2} & \sqrt{2/3}S^* & -B'^*/\sqrt{2} & \sqrt{2}Q' & \sqrt{3/2}B' & \sqrt{2}C'^* & P'+\Delta & 0 \\
-\sqrt{2/3}S & T^*/\sqrt{2} & -\sqrt{2}C'^* & \sqrt{3/2}B'^* & \sqrt{2}Q' & -B'/\sqrt{2} & 0 & P'+\Delta
\end{pmatrix}, \tag{13}$$

where

$$R'=E_c-E_{ss}a^2k^2,\quad S=-i2\sqrt{2}E_{sx}a(k_x+ik_y)\ ,$$
$$T=i8E_{sx}ak_z/\sqrt{6},\quad P'=E_v-[E_{xx}-(E_{zz}-E_{xx})/3]a^2k^2\ ,$$
$$Q'=-(E_{zz}-E_{xx})a^2(k^2-3k_z^2)/12,\quad B'=E_{xy}a^2(k_x-ik_y)k_z/\sqrt{3}\ ,$$
$$C'=-[(E_{zz}-E_{xx})(k_y^2-k_x^2)/4+iE_{xy}k_xk_y]a^2/\sqrt{3}\ .$$

To make connections between the bond-orbital interaction parameters and the $\mathbf{k}\cdot\mathbf{p}$ parameters, we block diagonalize the matrix $H(\mathbf{k})$ so that the conduction band and the valence bands are decoupled. The new Hamiltonian matrix correct to second order in $\mathbf{k}$ reads

$$H(\mathbf{k})=\begin{pmatrix}
R & 0 & 0 & 0 & 0 & 0 & 0 & 0 \\
0 & R & 0 & 0 & 0 & 0 & 0 & 0 \\
0 & 0 & P+Q & B & C & 0 & -B''/\sqrt{2} & -\sqrt{2}C'' \\
0 & 0 & B^* & P-Q & 0 & C & \sqrt{2}Q'' & \sqrt{3/2}B'' \\
0 & 0 & C^* & 0 & P-Q & -B & \sqrt{3/2}B''^* & -\sqrt{2}Q'' \\
0 & 0 & 0 & C^* & -B^* & P+Q & \sqrt{2}C'' & -B''^*/\sqrt{2} \\
0 & 0 & -B''^*/\sqrt{2} & \sqrt{2}Q'' & \sqrt{3/2}B'' & \sqrt{2}C''^* & P''+\Delta & 0 \\
0 & 0 & -\sqrt{2}C'' & \sqrt{3/2}B''^* & \sqrt{2}Q'' & -B''/\sqrt{2} & 0 & P''+\Delta
\end{pmatrix}, \tag{14}$$

where

$$R=E_c-E_{ss}a^2k^2+\left[2+\frac{E_g}{E_g+\Delta}\right]\lambda_4k^2/3\ ,$$
$$P=P'-\lambda_4k^2/3\ ,$$
$$Q=Q'-\lambda_4(k^2-3k_z^2)/6\ ,$$
$$B=B'+\lambda_4(k_x-ik_y)k_z/\sqrt{3}\ ,$$
$$C=C'+\lambda_4(k_x-ik_y)^2/\sqrt{12}\ ,$$
$$P''=P'-\frac{E_g}{E_g+\Delta}\lambda_4k^2/3\ ,$$
$$Q''=Q'-\frac{E_g}{E_g+\Delta}\lambda_4(k^2-3k_z^2)/6\ ,$$
$$B''=B'+\frac{E_g}{E_g+\Delta}\lambda_4(k_x-ik_y)k_z/\sqrt{3}\ ,$$
$$C''=C'+\frac{E_g}{E_g+\Delta}\lambda_4(k_x-ik_y)^2/\sqrt{12}\ .$$

Comparing the above matrix with the corresponding results of the $\mathbf{k}\cdot\mathbf{p}$ perturbation theory, we then established a one-to-one correspondence between the set of bond-orbital parameters [with the constraint (12)] and the set of $\mathbf{k}\cdot\mathbf{p}$ parameters. Such a relation is given in Table II in the column headed CVBM.

For systems with large spin-orbit splitting (Δ), we may eliminate the two split-off states $u_{1/2}^{1/2}$ and $u_{-1/2}^{1/2}$ by setting $\Delta=\infty$. It is worth pointing out that at $k_x=k_y=0$, states with different quantum numbers of J_z are decoupled [see (9)] and the present model becomes extremely simple. If we set $\Delta=\infty$ and $k_x=k_y=0$, the present model becomes essentially identical to the two-band model used in Refs. 13 and 28.

III. APPLICATIONS TO SUPERLATTICES

We now apply the bond-orbital models discussed in Sec. II to superlattices. An appropriate bond-orbital model is chosen for each participating material in the superlattice. The interactions between any two bond orbitals located in the same material are taken to be the same as those for the bulk. The interaction between two bond orbitals located in two different materials (i.e., the interaction across the interface) may be taken, for convenience, to be the average of the corresponding matrix elements in the two participating bulk materials. Since different choices of the interaction across the interface lead to different boundary conditions in determining the superlattice wave functions, the results will depend on how such interaction parameters are selected. In cases where sufficient experimental data are available for certain physical quantities that are sensitive to the boundary conditions, these interaction parameters across the interface may be appropriately treated as empirical parameters. Once the interactions among all bond orbitals in the superlattice are defined, one may proceed in several ways to calculate the electronic structures. For small-period superlattices, one can obtain all the electronic levels by a direct diagonalization method (the slab method).[5–8] For large-period superlattices, one can use the reduced Hamiltonian method[9,10] (applicable for any tight-binding model) to obtain the electronic levels in any desirable energy range. Because of the simplicity of the interaction matrix in the bond-orbital model, we find that the most convenient and powerful method to use is the transfer-matrix method.[29,30] Such a method can be applied to general situations in which the interaction parameters between bond orbitals vary from one atomic layer to another within the period of the superlattice. Thus, superlattices under external fields (electric, strain, modulation doping, etc.) and superlattices with composition variation (e.g., saw-tooth superlattices) can all be treated in the same way.

We describe the transfer-matrix method briefly below. For any kind of superlattice with period d, the superlattice state with wave vector $\mathbf{k}=(\mathbf{k}_\parallel,q)$ can be written as

$$\Psi_{\mathbf{k}_\parallel,q}=\sum_L e^{iqLd}\sum_{l=0}^{N-1} C_\alpha(l)\,|\,\mathbf{k}_\parallel,l,L;\alpha\rangle\ , \tag{15}$$

where L labels the superlattice unit cells (SUC's, l labels the atomic layer within a given SUC, and N is the number of atomic layers per SUC. Here an atomic layer contains all bulk unit cells in a lattice plane perpendicular to the growth direction. $|\,\mathbf{k}_\parallel,l,L;\alpha\rangle$ denotes a Bloch sum of α-like bond orbitals in the lth atomic layer in the Lth period associated with the in-plane wave vector $\mathbf{k}_\parallel$. Substituting $\Psi_{\mathbf{k}_\parallel,q}$ into the Schrödinger equation yields

$$\sum_L e^{iqLd}\sum_{l=1}^{N} C_\alpha(l)(H-E)\,|\,\mathbf{k}_\parallel,l,L;\alpha\rangle=0\ , \tag{16}$$

where H is the Hamiltonian for the superlattice and E is the energy of the superlattice state. Projecting (16) in bond orbitals located at atomic layer l leads to an equation relating the coefficients at layer $l+1$ to those at layers l and $l-1$, viz.,

$$C(l+1)=-[H^{(+)}(l)]^{-1}[H^{(0)}(l)C(l)+H^{(-)}(l)C(l-1)]\ ,$$

where $C(l)$ is a column vector whose components are the coefficients $C_\alpha(l)$ and $H^{(+)}$, $H^{(0)}$, and $H^{(-)}$ are matrices with elements

$$H^{(+)}_{\alpha,\alpha'}(l)=\langle\mathbf{k}_\parallel,l,L;\alpha\,|\,H\,|\,\mathbf{k}_\parallel,l+1,L;\alpha'\rangle\ ,$$

$$H^{(0)}_{\alpha,\alpha'}(l)=\langle\mathbf{k}_\parallel,l,L;\alpha\,|\,H\,|\,\mathbf{k}_\parallel,l,L;\alpha'\rangle-E\delta_{\alpha,\alpha'}\ ,$$

$$H^{(-)}_{\alpha,\alpha'}(l)=\langle\mathbf{k}_\parallel,l,L;\alpha\,|\,H\,|\,\mathbf{k}_\parallel,l-1,L;\alpha'\rangle\ .$$

We define a transfer matrix $T(l)$ as

$$T(l)=\begin{bmatrix}-[H^{(+)}(l)]^{-1}H^{(0)}(l) & -[H^{(+)}(l)]^{-1}H^{(-)}(l)\\ 1 & 0\end{bmatrix}.$$

Then we have

$$\begin{bmatrix}C(l+1)\\ C(l)\end{bmatrix}=T(l)\begin{bmatrix}C(l)\\ C(l-1)\end{bmatrix}. \tag{17}$$

Repeatedly applying (17) for l from 1 to N, we obtain

$$\begin{bmatrix}C(N+1)\\ C(N)\end{bmatrix}=T_N\begin{bmatrix}C(1)\\ C(0)\end{bmatrix}, \tag{18}$$

where $T_N=T(N)T(N-1)\cdots T(2)T(1)$. From the definition of the coefficients $C(l)$ in (15), we see that $C(l+N)=e^{iqLd}C(l)$. Thus

$$T_N\begin{bmatrix}C(1)\\ C(0)\end{bmatrix}=e^{iqLd}\begin{bmatrix}C(1)\\ C(0)\end{bmatrix}. \tag{19}$$

Since T_N is a function of the energy E, the eigenvalue equation (19) can be solved to find the dispersion relation (E versus q).

IV. RESULTS

We shall illustrate the use of the method by calculating the subband structure of GaAs-Al_xGa_{1-x}As and InAs-GaSb superlattices. For GaAs-Al_xGa_{1-x}As systems, we shall use the valence-band model (VBM) (with infinite

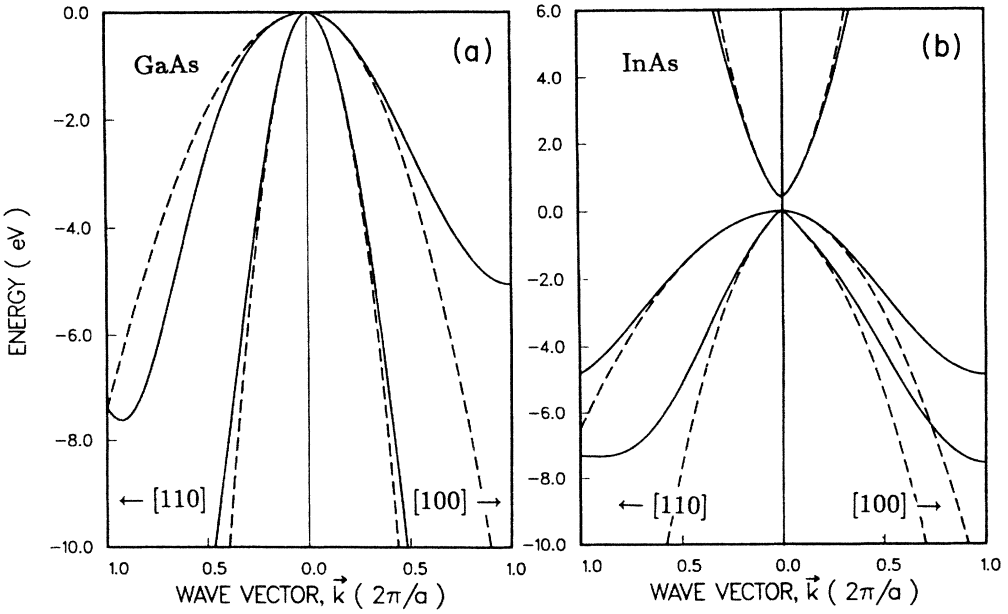

FIG. 1. (a) Valence-band structures of GaAs obtained in the VBM (solid line) and in the **k·p** theory (dashed line). (b) Band structures of InAs obtained in the CVBM (solid line) and in the **k·p** theory (dashed line).

spin-orbit interaction) to examine the valence-subband structures. The conduction-subband structures are trivial and they can be obtained by a one-band model (e.g., one *s*-like bond orbital per unit cell). For InAs-GaSb superlattices, we shall use the coupled conduction–valence-band model with infinite spin-orbit interaction.

Figure 1(a) shows the bulk valence-band structures of GaAs obtained by the VBM (solid curves) and by the **k·p** model (dashed curves). The Luttinger parameters used are the same as in Ref. 21. Figure 1(b) shows the bulk valence-band structures of InAs obtained by the CVBM (solid curves) and by the **k·p** model (dashed curves). The Luttinger parameters used are the same as in Ref. 27 and the band gap is chosen to be 0.41 eV.[31] The **k·p** model result is obtained by diagonalizing the upper left 6×6 block of (13). As expected, the band structures obtained from the bond-orbital model and the **k·p** model are nearly identical for small values of **k**. For large values of **k**, the bond-orbital model gives more satisfactory results than the **k·p** model.

Figure 2 shows the valence-subband structures of a (30,20) GaAs-$Al_{0.1}Ga_{0.9}As$ superlattice for wave vectors (**k**) along $[00\zeta]$ (the growth direction), $[\zeta00]$ (the in-plane direction), and $[\zeta01]$ ($\zeta=0-1$). The units for wave vectors are π/d, where d is the width of the superlattice unit cell in the growth direction. Here the symbol (30,20) indicates that the superlattice has 30 GaAs atomic layers and 20 $Al_{0.1}Ga_{0.9}As$ atomic layers per superlattice unit cell. The symbols HH*n* and LH*n* denote the *n*th heavy-hole and light-hole subbands, respectively. The valence-band parameters for AlAs are taken from Ref. 27, and the valence-band discontinuity is chosen to be 31% of the band-gap difference for GaAs and AlAs.[32] The virtual-crystal approximation is used to treat the $Al_{0.1}Ga_{0.9}As$ alloy. The small (10%) Al mole fraction is chosen for the alloy layer, because this allows substantial energy dispersion in the growth direction even with a thick barrier. It has been demonstrated recently that interesting saddle-point exciton resonances can show up in the absorption spectra of superlattices with large subband dispersion in the growth direction.[33] From the experimental point of view it is desirable to keep both the well and barrier thick in order to minimize the fractional error in the layer thickness. In Fig. 2, a few interesting features are noted. In a superlattice with nearly decoupled wells, the sub-

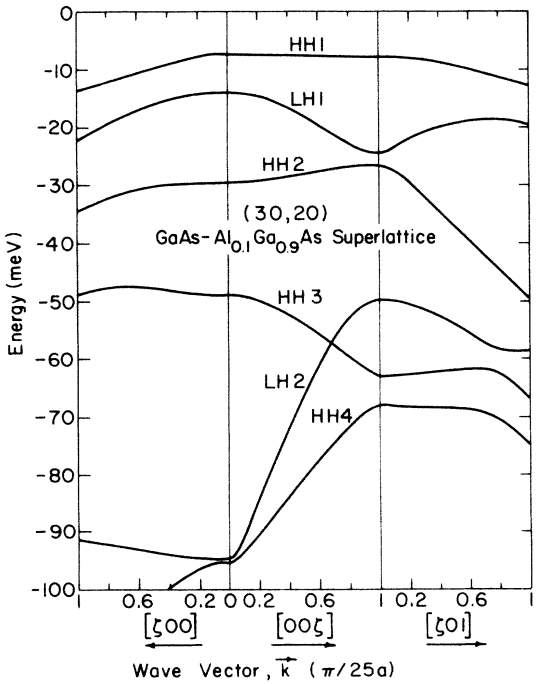

FIG. 2. Valence-subband structures of a (30,20) GaAs-$Al_{0.1}Ga_{0.9}As$ superlattice obtained in the VBM.

band dispersion along the growth direction is expected to be small and the subband dispersion along [ζ00] (with k_z at zone center) should be quite similar to that along [ζ01] (with k_z at zone boundary). In the present case, we have substantial dispersion in the growth direction, and the [ζ00] and [ζ01] subband dispersions are quite different. In particular, the first light-hole band (LH1) has positive curvature along [ζ01], but negative curvature along [ζ00]. Note that the LH1 band typically has positive curvature in GaAs-$Al_xGa_{1-x}As$ quantum wells with thickness greater than 50 Å.[21] Another interesting feature is that the HH3 and LH2 bands cross at some finite k_z; thus, the HH3 band has higher energy than the LH2 band along [ζ00] and the opposite is true along [ζ01].

As another example, we show in Fig. 3 the subband structure of a (10,10) InAs-GaSb superlattice along [ζ00], [00ζ], and [ζ01]. The wave vectors are again measured in units of π/d. The band parameters for bulk InAs and GaSb are taken from Ref. 27. The band discontinuity ΔE (valence-band maximum of GaSb minus conduction-band minimum of InAs) is taken to be 0.1 eV.[34] Because this is a type-II superlattice,[28] the superlattice states in general contain admixtures of bulk conduction-band and valence-band states. However, for the (10,10) case, the mixing of the conduction and valence band is rather weak, because the superlattice conduction and light-hole states are still well separated in energy (larger than 0.4 eV). In the wider-thickness case, the mixing can be much stronger. The valence-subband structure is qualitatively similar to that of the GaAs-$Al_{0.1}Ga_{0.9}As$ superlattice shown in Fig. 2, with the exception that in the InAs-GaSb superlattice the LH1 and HH2 bands cross at some finite k_z, causing a reverse ordering of LH1 and HH2 in the [ζ01] direction. Comparing Fig. 3 with a previous calculation[34] within the empirical tight-binding model, we find that the major difference between the two calculations (besides the difference in bulk band parameters) is the lack of spin splitting in the present calculation. In the present bond-orbital model, the superlattice has reflection symmetry with respect to the center of the InAs or GaSb layer, whereas in the tight-binding model (and the realistic system) the reflection symmetry does not exist. For larger superlattice unit cell, the effect of the asymmetry and thus the spin splitting would be greatly reduced. Furthermore, we note that for wave vectors along the growth direction the heavy-hole-derived states and light-hole-derived states are completely decoupled in the bond-orbital model (also in the $\mathbf{k}\cdot\mathbf{p}$ model); thus a heavy-hole subband and a light-hole subband can cross each other, as can be seen in the middle panels of Figs. 2 and 3. However, in the more tight-binding model, the heavy-hole and light-hole subbands are coupled for a general value of q (the z component of superlattice wave vector); thus anticrossing behavior is expected (see Fig. 13 of Ref. 34). This qualitative difference is due to the artificially high symmetry of the bond-orbital model which treats the crystal as if it is the underlying Bravais lattice. For finite value of k_z, the realistic zinc-blende crystal has a symmetry group C_{2v}, whereas the face-centered-cubic lattice has a symmetry group C_{4v}.[35] For the C_{2v} group, there is only one double-group irreducible representation;[36] thus, no two subbands should cross each other. For the C_{4v} group, there are two double-group irreducible representations;[36] thus, crossing of two subbands of different symmetries is possible.

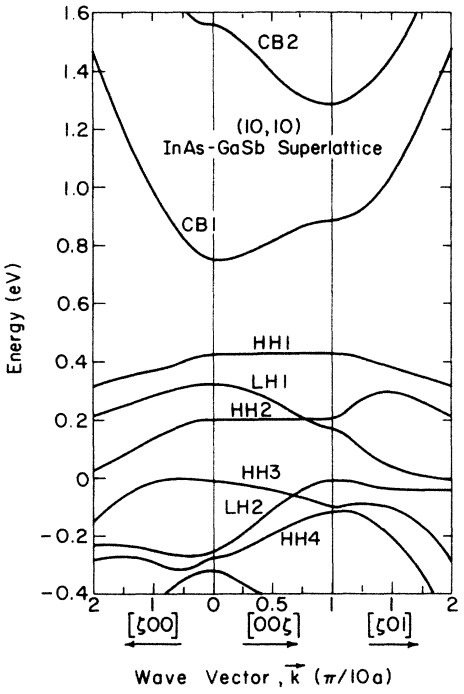

FIG. 3. Subband structures of a (10,10) InAs-GaSb superlattice obtained in the CVBM.

ACKNOWLEDGMENTS

This work was supported in part by the U.S. Office of Naval Research (ONR) under Contract No. N00014-81-K-0430. The computing facility provided by the University of Illinois, Materials Research Laboratory, under National Science Foundation (NSF) Grant No. NSF-DMR-86-12860 is gratefully acknowledged.

[1]L. Esaki and R. Tsu, IBM J. Res. Dev. **14**, 61 (1970).
[2]E. Caruthes and P. J. Lin-Chung, Phys. Rev. Lett. **39**, 1543 (1977).
[3]W. Andreoni, A. Baldereschi, and R. Car, Solid State Commun. **27**, 821 (1978).
[4]M. A. Gell, D. Ninno, M. Jaros, and D. C. Herbert, Phys. Rev. B **34**, 2416 (1986).
[5]J. N. Schulman and T. C. McGill, Phys. Rev. Lett. **39**, 1680 (1977); Appl. Phys. Lett. **34**, 663 (1979).
[6]R. N. Nucho and A. Madhukar, J. Vac. Sci. Technol. **15**, 1530

(1978).
[7]A. Madhukar, N. V. Dandekar, and R. N. Nucho, J. Vac. Sci. Technol. **16**, 1507 (1979).
[8]G. C. Osbourn, J. Appl. Phys. **53**, 1586 (1982).
[9]J. N. Schulman and Y. C. Chang, Phys. Rev. B **24**, 4445 (1981); **27**, 2346 (1983).
[10]Y. C. Chang and J. N. Schulman, J. Vac. Sci. Technol. **21**, 540 (1982).
[11]S. Krishnamurthy and J. A. Moriarty, Phys. Rev. B **32**, 1027 (1985).
[12]G. A. Sai Halasz, R. Tsu, and L. Esaki, Appl. Phys. Lett. **30**, 651 (1977).
[13]G. Bastard, Phys. Rev. B **25**, 7584 (1982).
[14]C. Mailhoit, D. L. Smith, and T. C. McGill, J. Vac. Sci. Technol. B **2**, 371 (1984).
[15]D. L. Smith and C. Mailhiot, Phys. Rev. B **33**, 8345 (1986); C. Mailhiot and D. L. Smith, *ibid.* **33**, 8360 (1986).
[16]W. Pötz, W. Porod, and D. K. Ferry, Phys. Rev. B **32**, 3686 (1985).
[17]D. A. Broido and L. J. Sham, Phys. Rev. B **31**, 888 (1985).
[18]A. Fasolino and M. Altarelli, in *Two-Dimensional Systems, Heterostructures, and Superlattices*, edited by G. Bauer, F. Kucher, and H. Heinrich (Springer-Verlag, New York, 1984).
[19]M. Atarelli, Phys. Rev. B **32**, 5138 (1985).
[20]G. D. Sanders and Y. C. Chang, Phys. Rev. B **32**, 5517 (1985).
[21]G. D. Sanders and Y. C. Chang, Phys. Rev. B **35**, 1300 (1987).
[22]W. A. Harrison, Phys. Rev. B **8**, 4487 (1973).
[23]J. C. Slater and G. F. Koster, Phys. Rev. **94**, 1498 (1954).
[24]E. O. Kane, J. Phys. Chem. Solids **1**, 83 (1956).
[25]J. C. Hensel and G. Feher, Phys. Rev. **129**, 1041 (1963).
[26]J. M. Luttinger and W. Kohn, Phys. Rev. **97**, 869 (1956).
[27]P. Lawaetz, Phys. Rev. B **4**, 3460 (1971).
[28]G. A. Sai Halasz, L. Esaki, and W. A. Harrison, Phys. Rev. B **18**, 2812 (1978).
[29]E. J. Mele and J. D. Joannopoulous, Phys. Rev. B **17**, 1816 (1978).
[30]D. H. Lee and J. D. Joannopoulous, Phys. Rev. B **23**, 4988, 4977 (1981).
[31]E. Adachi, J. Phys. Soc. Jpn. **24**, 1178 (1968).
[32]D. J. Wolford, T. F. Keuch, J. A. Bradley, M. A. Gell, D. Ninno, and M. Jaros, J. Vac. Sci. Technol. B **4**, 1043 (1986).
[33]H. Chu and Y. C. Chang, Phys. Rev. B **36**, 2946 (1987).
[34]Y. C. Chang and J. N. Schulman, Phys. Rev. B **31**, 2069 (1985).
[35]See, for example, N. W. Ashcroft and N. D. Mermin, *Solid State Physics* (Saunders College, Philadelphia, 1975), Chap. 7.
[36]See for example, G. F. Koster, J. O. Dimmock, R. G. Wheeler, and H. Statz, *Properties of the Thirty-two Point Groups* (Cambridge University Press, Cambridge, 1963).